Chemoprevention of Lung Squamous Cell Carcinoma in Mice by a Mixture of Chinese Herbs

Yian Wang,[1] Zhongqiu Zhang,[1] Joel R. Garbow,[2] Doug J. Rowland,[2] Ronald A. Lubet,[3] Daniel Sit,[4] Francis Law[4] and Ming You[1]

Abstract Antitumor B (ATB) is a Chinese herbal mixture of six plants. Previous studies have shown significant chemopreventive efficacy of ATB against human esophageal and lung cancers. We have recently developed a new mouse model for lung squamous cell carcinomas (SCC). In this study, lung SCC mouse model was characterized using small-animal imaging techniques (magnetic resonance imaging and computed tomography). ATB decreased lung SCC significantly (3.1-fold; $P < 0.05$) and increased lung hyperplastic lesions by 2.4-fold ($P < 0.05$). This observation suggests that ATB can block hyperplasia from progression to SCC. ATB tissue distribution was determined using matrine as a marker chemical. We found that ATB is rapidly absorbed and then distributes to various tissues including the lung. These results indicate that ATB is a potent chemopreventive agent against the development of mouse lung SCCs.

Introduction

Lung cancer is the leading cause of cancer death in the world and is one of the most preventable diseases (1). Cancer chemoprevention uses natural or synthetic agents to reverse, suppress, or prevent carcinogenic progression. Cancer chemopreventive agents can be classified into two major groups, blocking agents and suppressing agents. As the population of former smokers is markedly growing, chemopreventive agents are urgently needed. Agents such as α-tocopherol, β-carotene (2), aspirin (2), retinol (3–5), isotretinoin (6), N-acetylcysteine (7), and anethole dithiolethione (8) have been tested in clinical trials in smokers. Unfortunately, there are no chemoprevention agents for lung cancer that have clearly shown clinical benefit. There are a variety of agents that have shown promise in animal studies including glucocorticoids, epidermal growth factor receptor inhibitors, retinoid X receptor agonists, tea polyphenols, deguelin, and the herbal mixture Antitumor B (ATB; refs. 9, 10–12). Among these, only ATB has had success in human trials (13). ATB, a Chinese herbal mixture, is a botanical agent composed of six Chinese herbs: *Sophora tonkinensis, Polygonum bistorta, Prunella vulgaris, Sonchus brachyotus, Dictamnus dasycarpus*, and *Dioscorea bulbifera* (13). Previous reports have shown that ATB treatment reduced cancer development by 50% in patients with marked esophageal dysplasia (13). In a chemically induced lung adenocarcinoma model, we showed that ATB caused a significant reduction in lung tumor multiplicity and tumor load by 40% and 70%, respectively (10).

Magnetic resonance imaging (MRI) and computed tomography (CT) are powerful imaging modalities for characterizing animal systems and animal models of disease. *In vivo* MRI permits a wide variety of noninvasive, nondestructive longitudinal studies not possible with other analytic methods. The lung presents unique challenges for MRI, requiring the development of new and innovative methods (14, 15). Among the complicating factors for the study of lungs by ^{1}H MR methods are as follows: (*a*) low tissue density and low water content within the lung, severely limiting signal-to-noise; (*b*) variations in magnetic susceptibility associated with the many air-tissue interfaces of the alveoli and bronchioles result in short T2* and T2 relaxation times; and (*c*) respiratory and cardiac motions lead to significant image blurring in the absence of motion-synchronized data acquisition. Using respiratory-gated MRI methods, we have recently shown the detection of submillimeter lung lesions in mice treated with the carcinogen, benzo(*a*)pyrene (14). Micro-CT is also a noninvasive, nondestructive imaging technique. The small size of mice limits contrast between tissues of similar density without the use of contrast enhancement agents; however, micro-CT can take advantage of the high contrast between low-density

Authors' Affiliations: [1]Departments of Surgery and The Alvin J. Siteman Cancer Center, Washington University School of Medicine; Department of [2]Radiology, Washington University School of Medicine, St. Louis, Missouri; [3]Chemoprevention Branch, National Cancer Institute, Bethesda, Maryland; and [4]Department of Biological Sciences, Simon Fraser University, Burnaby, BC, Canada

Received 12/2/08; revised 3/18/09; accepted 3/24/09.

Grant support: United States Public Health Service Grants R01 AT003203 & N01-CN-25104 (M. You), an NIH/National Cancer Institute Small Animal Imaging Resource Program grant (R24 CA83060); and the Alvin J. Siteman Cancer Center at Washington University in St. Louis, a National Cancer Institute Comprehensive Cancer Center (P30 CA91842).

Note: Supplementary data for this article are available at Cancer Prevention Research Online (http://cancerprevres.aacrjournals.org/).

Requests for reprints: Ming You, Washington University, 660 South Eulcid Avenue, 4950 Children's Place, St. Louis, MO 63110. Phone: 314-362-9294; Fax: 314-362-9366; E-mail: youm@wudosis.wustl.edu.

©2009 American Association for Cancer Research.

doi:10.1158/1940-6207.CAPR-09-0052

Downloaded from cancerpreventionresearch.aacrjournals.org on January 28, 2022. © 2009 American Association for Cancer Research.

lung tissue and high-density cancer tissue without contrast enhancement.

Recently, we reported a chemically induced model for squamous cell carcinomas (SCC) of the lung in mice (16). The objectives of the present study are to further characterize lung SCC mouse model using small-animal imaging techniques (MRI and CT) and to evaluate the effect of ATB on the development of lung SCC in mice. Our results show that dietary ATB causes a significant inhibition in the development of mouse lung SCC. To our knowledge, this is the first report of significant efficacy against lung tumors in a mouse lung SCC model.

Materials and Methods

Reagents and animals

Benzo(*a*)pyrene, tricaprylin, and acetone were purchased from Sigma. Vinyl carbamate and N-nitroso-trischloroethylurea (NTCU) were purchased from Toronto Research Chemicals, Inc. The putative chemopreventive agent, ATB, was purchased from the Cancer Institute, the Chinese Academy of Medical Sciences (Beijing, China). Female A/J mice were received from The Jackson Laboratory at age 6 wk. Animals were quarantined for 1 wk and housed with wood chip bedding in environmentally controlled, clean-air rooms with a 12-h light-dark cycle and relative humidity of 50%. Drinking water and diet were supplied *ad libitum*. The study was approved by the Washington University's Institutional Animal Care and Use Committee.

MRI

Respiratory-gated, spin-echo MR images of mice were collected in an Oxford Instruments 4.7 tesla, 40-cm bore magnet. The magnet is equipped with Magnex Scientific actively shielded, high-performance (10 cm inner diameter, 60 G/cm, 100-μs rise-time) gradient coils and is interfaced with a Varian NMR Systems INOVA console. All data were collected using a Stark Contrast 2.5-cm birdcage radiofrequency coil. Before the imaging experiments, mice were anesthetized with isoflurane and were maintained on isoflurane/O2 (1-1.5% v/v) throughout data collection. Animal core body temperature was maintained at 37 ± 1°C by circulation of warm air through the bore of the magnet. Approximately 500 μL of Omniscan (Gadodiamide; GE Healthcare) contrast agent, diluted 1:10 in saline, was injected i.p. immediately before placing the animal in the magnet. During the imaging experiments, the respiration rates for all mice were regular and 2 s^{-1}. Synchronization of MR data collection with animal respiration was achieved with a home-built respiratory-gating unit (14), and all images were collected during postexpiratory periods. Imaging parameters are repetition time of 3 s, echo time of 20 ms, 2.5 cm field of view, and slice thickness of 0.5 mm.

Micro-CT

Mice were anesthetized in a similar fashion to that of the MR studies. Animal temperature was regulated at ambient room air. Pairs of mice were imaged on a microCAT-II scanner (Seimens-CTI Concorde, Inc.). Scans were done at either low (adenocarcinoma) or high (SCC) resolution. Low-resolution images used an X-ray source energy of 80 kvP with a 200 ms exposure time and 400 view angles over 360 degrees. High-resolution images used X-ray source energy of 60 kvp with a 500 ms exposure time and 600 view angles. Adenocarcinoma images were reconstructed at low resolution (200 × 200 × 96 μm), and SCC images were reconstructed at 96 μm istotropic voxel size.

Animal bioassays using a chemically induced SCC model

A/J mice at age 6 to 8 wk were randomized into two groups. All mice were treated topically with 0.04 mol/L NTCU in 100-microliter drop, twice a week, with a 3.5-d interval for 22 wk (16). Two weeks after the start of NTCU treatment, mice in group 1 were fed AIN-76A Purified Diet # 100 000 (Dyets, Inc.) and mice in group 2 were fed with the same diet plus 250 g/kg ATB. Food was changed every other day. Twenty-four weeks after the initial treatment of NTCU, mice were terminated by CO2 asphyxiation. Lungs were fixed in Tellyesniczky's [90% ethanol (70% v/v), 5% glacial acetic acid, 5% formalin (10% v/v buffered formalin)] solution overnight and stored in 70% ethanol for histopathologic evaluation. Unlike the mouse lung adenomas/adenocarcinomas, mouse SCC dose not form visible solid nodules on the surface of the lung. Serial tissue sections (4-μm each) were made from formalin-fixed lungs, and 1 in every 20 sections (~100 μm apart) was stained with H&E and examined histologically under a light microscope to establish tumor multiplicity and the types of lesions (invasive SCC, SCC *in situ*, or bronchial hyperplasia/metaplasia).

Statistical analysis

We hypothesized that chemically induced lung tumors are more likely to occur in the carcinogen control group than in the treatment groups. To test this hypothesis, the Student's *t* test was used. The data were obtained from the carcinogen control groups and different treatment groups in each experiment. We applied square-root transformation of tumor numbers because the original data did not follow normal distribution. The transformed data were of normal distribution (data not shown). Accordingly, the Student's *t* test was used to test the differences between the control groups and the treatment groups.

Matrine tissue distribution in mice

Thirty-six A/J female mice weighing ~20 grams each were randomly assigned into two groups. The mice were fed with feeds mixed with either 20% or 30% of ATB for 4 wk. Three mice were removed from each group and sacrificed at predetermined time points (0, 2, 4, 7, 14, and 28 d) during the experiment. A blood sample was taken from each mouse immediately and was centrifuged at 3,000 rpm for 5 min to collect the plasma. The liver, lung, kidney, heart, and spleen also were removed from the carcass; they were snap-frozen in liquid nitrogen. All tissue samples were stored in a −70°C freezer until analysis.

The tissue samples were thawed at room temperature. About 0.3 gram of each tissue was weighed and then homogenized with 0.9 mL of distilled water in a Kinemetica GmbH PCU-2-110 tissue homogenizer. The liver and kidney were homogenized individually. The lung, spleen, and heart from three different mice were combined before being homogenized because of the small organ sizes. The final volumes of the homogenates were recorded. Extraction and measurement of matrine were conducted according to Sit et al. (17) with modification. Briefly, a 1-mL aliquot of each tissue homogenate was mixed with 50 μL of a deuterated matrine solution (5 μg/mL) in a 10-mL screw capped glass centrifuged tube. The deuterated matrine was used as an internal standard of the assay. NaOH (0.5 mL, 1 mol/L) was added to make the content of the centrifuge tube alkaline. The mixture was then extracted with 3 mL of toluene/butanol (v/v 7:3) on a mechanical shaker. After the centrifuge tube was centrifuged to separate the layers, the organic layer was removed and put into a new glass centrifuge tube containing 0.5 mL of 0.25 mol/L HCl. The content in the centrifuge tube was mixed, centrifuged, and the organic layer was discarded. The remaining aqueous layer was mixed with 0.5 mL of 1 mol/L NaOH before being extracted by 300 μL toluene/butanol (v/v 9:1). The organic layer was removed and analyzed by a gas chromatograph/mass spectrometer using the selective ion monitoring mode. The *m/z* 248 and *m/z* 250 ions were used to monitor matrine and deuterated matrine, respectively. Matrine concentration in a tissue sample was calculated from the area ratio of *m/z* 248:*m/z* 250, the tissue weight, and the homogenate volume (17).

Downloaded from cancerpreventionresearch.aacrjournals.org on January 28, 2022. © 2009 American Association for Cancer Research.

Results

Histopathology of mouse lung SCC and human lung SCC

Under light microscopy, normal bronchi are seen as a single layer of bronchial epithelial cells (Fig. 1A, *a-1*).Upon NTCU treatment, the single layer bronchial epithelial cells are replaced with multiple layers of cells (hyperplasia) with increased production of keratin (Fig. 1A, *a-2*).

Squamous metaplasia is seen locally (Fig. 1A, *b*). The lung SCC consists of large, flattened, and stratified cells with intracytoplasmic keratin/keratin pearls (Fig. 1B, *arrowhead*) and/or intercellular bridges (Fig. 1A, *d, arrows*), which is a less common phenomenon in mouse lung SCC. Anisokaryosis is another dominate feature in SCC tumor cells (Fig. 1A, *d*). Most SCC arises centrally within the bronchi at different levels, including main, lobar, segmental, or subsegmental bronchi. The tumor cells can break through the wall of bronchus and invade into lung parenchyma (Fig. 1A, *c*). As shown in Fig. 1B, there is a remarkable similarity in the progressive morphologic changes during the development of lung SCCs between mice and humans. Multistage development of SCC in human

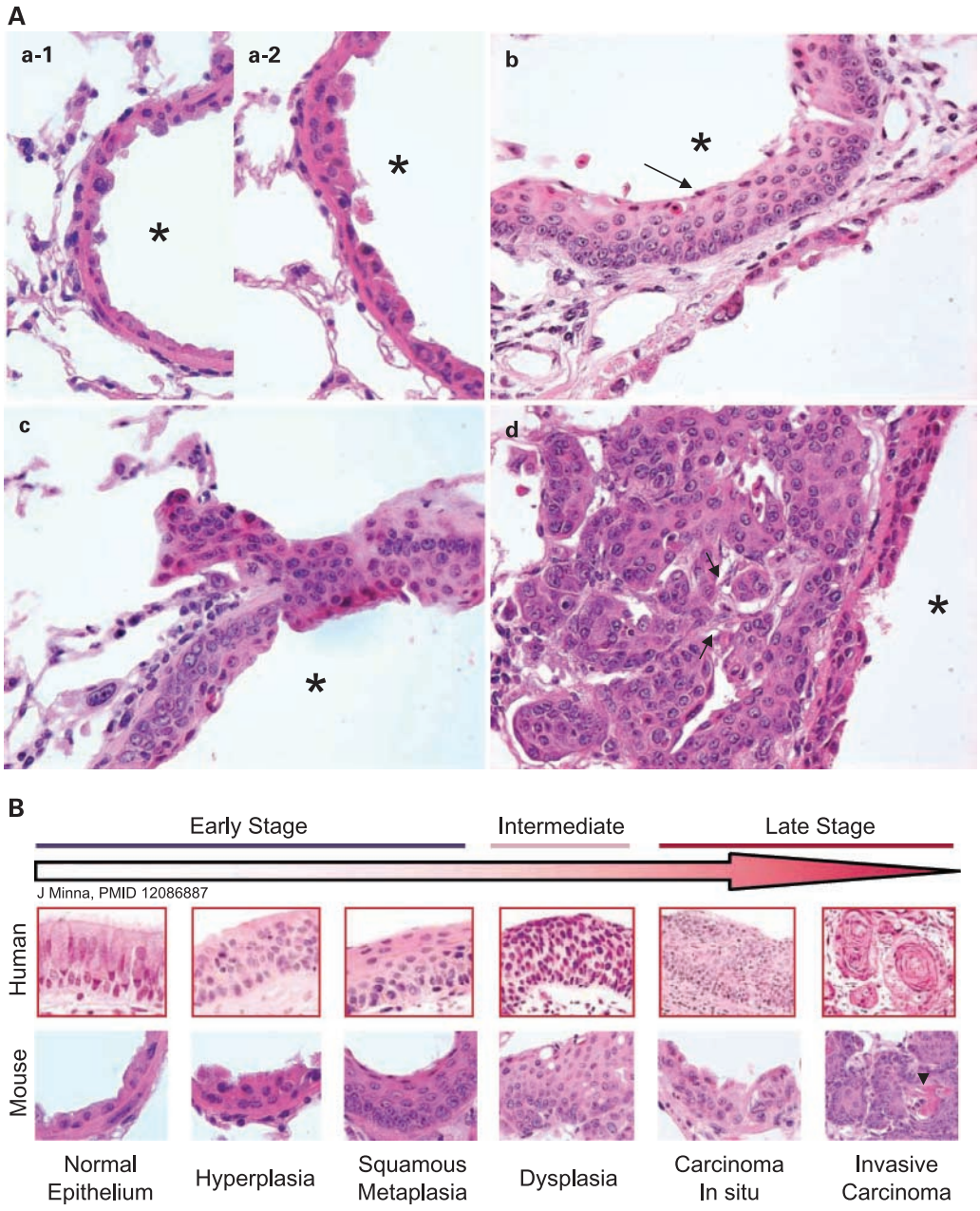

Fig. 1. Histopathology of human and mouse lung SCC. *A,* histopathology of mouse lung squamous hyperplasia, metaplasia, carcinomas *in situ*, and carcinoma is shown. *B, top,* squamous lesions of human lung [adapted from Minna et al. (18)]; *bottom,* similar lesions in mouse lung.

Downloaded from cancerpreventionresearch.aacrjournals.org on January 28, 2022. © 2009 American Association for Cancer Research.

can be seen histologically from normal epithelium, to early stage (hyperplasia, squamous metaplasia), intermediate stage (dysplasia), to late stage (carcinoma *in situ*, and invasive tumor; ref. 18). Similarly, serial lesions in mouse lung SCC development can easily be identified because of the uniform appearance of the normal bronchial epithelium, with a single layer of columnar cells, is markedly different from the hyperplasia of bronchial epithelium with increased cell number and a multilayered bronchial epithelium (Fig. 1). Bronchial epithelium is replaced by a stratified, keratinized, squamous epithelium in squamous metaplasia. Dysplasia is seen by increased epithelial cell layers and increased nucleus/cytoplasm ratio. In the carcinoma *in situ*, bronchiolar epithelial cells become atypical with irregular shape, increased nucleus/cytoplasm ratio, with mitosis, loss of orderly differentiation through the entire thickened epithelium. The bronchiole basement membrane is intact with no tumor cells in the surrounding stroma. In the invasive SCC, the cancerous cells are not only disordered throughout the entire thickness of the lining, but they invade the tissue underlying the bronchiole basement membrane into the surrounding stroma. The typical SCC can be seen, including keratin pearls, multiple nuclei, and increasing mitotic index. The normal architecture of the lung is disrupted. Cords and nests of tumors can be seen in the subepithelial stroma.

Imaging analysis of mouse lung SCC

We characterized our mouse lung SCC model using small-animal imaging techniques (MRI and CT) and compared this with the imaging using the well-characterized A/J mouse lung adenocarcinoma model. The images were correlated with gross (Fig. 2A) and histopathologic examinations of the tumors (Fig. 1). Both lung adenocarcinomas and SCCs were successfully detected using both MRI and micro-CT. Figure 2B shows a series of contiguous coronal, respiratory-gated spin-echo images of one mouse with adenocarcinomas and two mice with SCCs, at early and advanced stages of disease, respectively. As described in the Introduction, lungs present several unique challenges to study by MRI. However, the very factors that make it difficult to image healthy lung parenchyma, including low tissue density, low water content, and variations in magnetic susceptibility within the lung, in fact aid in the detection of tumors by increasing the contrast between healthy and pathologic tissue. Under the selected experimental conditions, the MR images of healthy mouse lung parenchyma are completely dark, whereas signals attributable to the heart and its major blood vessels are suppressed because of flow effects and cardiac motion (electrocardiograph gating was not used in this study). The bright spots visible in Fig. 2B are attributable to lung tumors compared with the absence of signal in healthy lungs. As seen in Fig. 2B, the MR images of adenocarcinomas show well-defined nodules that are distributed randomly throughout the lungs. In contrast, the images of early stage SCCs show nodules that are centrally located along the trachea, whereas diffuse tumor tissue fills the lungs in the later stages of the disease. These results were further confirmed by micro-CT scans (Fig. 2C). Although tumor number of adenocarcinomas by both MRI and micro-CT correlated positively with tumor number by necropsy and histopathology, the tumor counts of SCCs from histopathology are difficult to compare. The images of SCCs from both MRI and micro-CT showed lesions that are rather continuous than discreet. To our knowledge, we report for the first time the *in vivo* detection of primary lung SCCs at a submillimeter level, correlated with histopathology in mice.

Effect of ATB on mouse model of lung SCC

In this study, ATB did not cause any symptoms of toxicity or apparent signs of ill health, nor have any significant affect on body weight in mice when given at a dose of 250 gram/kg. As shown in Fig. 3, in control NTCU-animals, the distributions of lesions are as follows: normal (37.6 ± 8.7%), hyperplasia (18.7 ± 2.8%), metaplasia (9.4 ± 1.9%), carcinoma *in situ* (8.6 ± 2.0%), and SCC (23.9 ± 8.3%). In animals treated with ATB, the distributions of lesions are follows: normal (31.0 ± 5.8%), hyperplasia (45.4 ± 4.9%; $P < 0.05$), metaplasia (6.7 ± 1.6%), carcinoma *in situ* (9.3 ± 2.8%), and SCC (7.6 ± 3.5%; $P < 0.05$). ATB decreases lung SCC development significantly (3.1-fold; $P < 0.05$). At the same time, the percentages of the hyperplastic bronchioles are increased by 2.4-fold ($P < 0.05$). This observation indicates that ATB can block the progression of hyperplasia to SCC. An important observation in the present study is that ATB inhibits the progression of lung SCC.

Next, we determined the accumulation of ATB in the lung. Because ATB is composed of six Chinese herbs, it would be difficult if not impossible to examine the disposition of each ATB component in the lung tissue. We have chosen matrine as a marker chemical or tracer of ATB because matrine is one of the most abundant ATB components (19). In fact, matrine has been used as an indicator of ATB consistency between different batches by us and other groups (19). The product produced for human consumption is standardized to matrine content with each tablet containing 1.2 to 1.7 mg of matrine (19). Moreover, matrine has been shown to possess anticancer activities and appears to be a reasonable substitute for examining the biodistribution of ATB (20, 21). Figure 4 shows that matrine is rapidly absorbed by mice fed with 20% or 30% of ATB in their foods. Thus, matrine could be detected in the mouse tissues at day 2 (the earliest time point of sampling) after initiating the feeding study. The matrine concentration-time profiles were found to peak in mouse tissues at day 7, however differed in the amounts in each tissue. (Fig. 4). Little to no matrine could be detected in the heart of mice treated with 20% ATB. Matrine also was not detected in the spleen of mice treated either with 20% or 30% ATB. Because only three plasma samples in the 30% ATB treatment group had matrine levels significantly higher than the limit of quantification of the analytic method (~13 ng/mL), it was not possible to derive any meaningful pharmacokinetic parameters from the plasma concentration-time curve. All together, these results suggest that only a small fraction of the matrine consumed by the mice is absorbed. Similar results have been observed in the rat and human (19). Although the amount of matrine or ATB absorbed is small, the absorption does occur quickly and then distributes to the various animal tissues. Lung is an important site of ATB disposition.

Discussion

In this study, we show that ATB is effective in chemoprevention of lung tumorigenesis in a mouse model of lung SCCs. The results, showing efficacy of ATB against the

Downloaded from cancerpreventionresearch.aacrjournals.org on January 28, 2022. © 2009 American Association for Cancer Research.

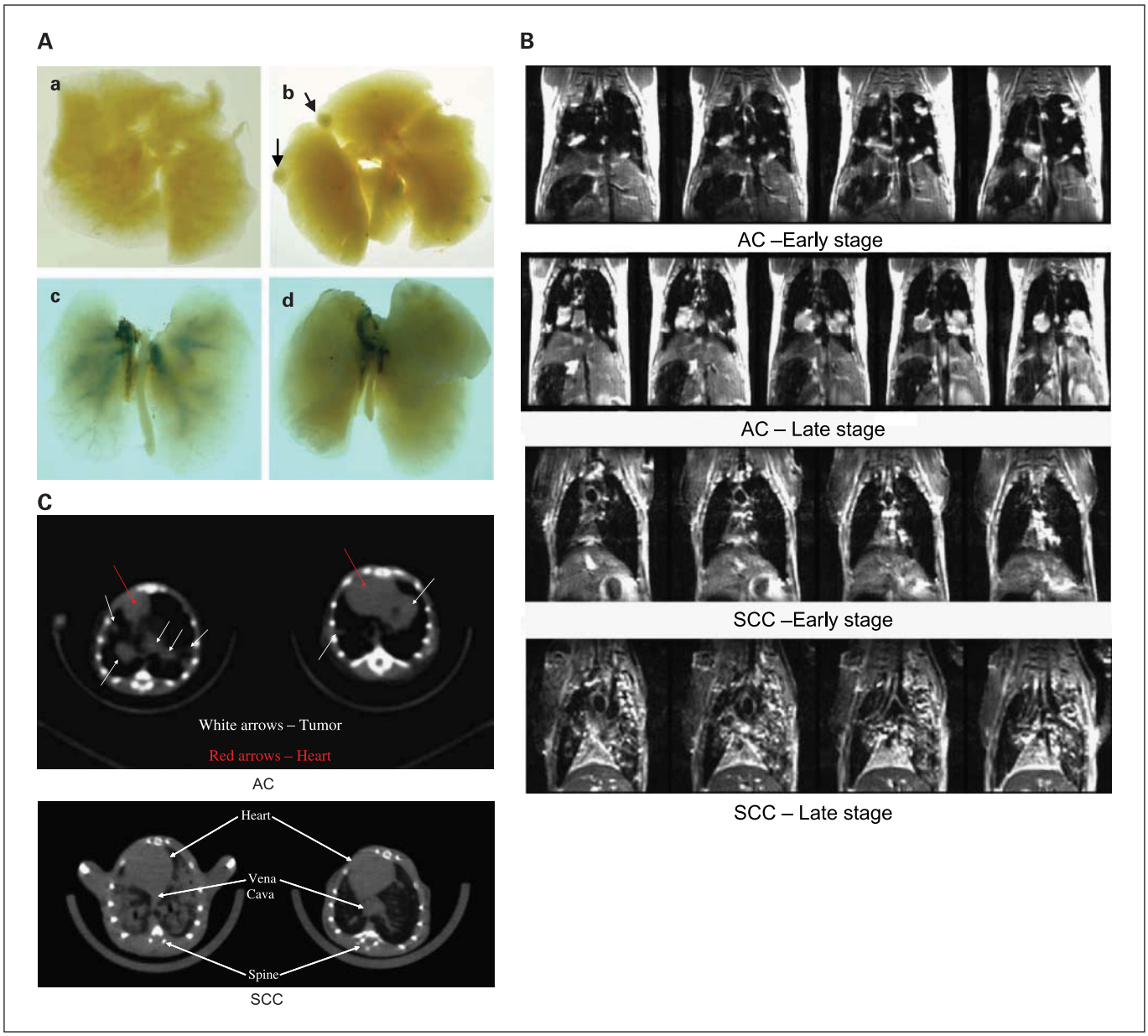

Fig. 2. Imaging mouse lung adenocarcinomas and SCC. *A,* gross appearance of mouse normal lungs. *a* and *c,* lung with adenoma/adenocarcinoma (*AC*); *b* and *d,* lung with SCC. *B,* MRI. Contiguous coronal slices, ventral to dorsal, from a series of respiratory-gated, spin-echo magnetic resonance (*MR*) images of a mouse with adenocarcinoma and two mice with SCC, at early and advanced stages of disease, respectively. Images were collected with repetition time of 3 s, echo time of 20 ms, field of view of 2.5 cm, slice thickness of 0.5 mm, and 128 × 128 data matrix, four averages. The images of healthy mouse lung parenchyma collected under these experimental conditions are completely black and the bright spots visible in these images are attributable to lung tumors. These images were collected following an i.p. injection of Omniscan contrast agent. Although these images are not heavily T1 weighted, the addition of contrast agent does increase the brightness of tumors within the lung. *C,* micro-CT. Transaxial slices of mouse lungs for adenocarcinoma (*top*) and SCC (*bottom*) tumor-bearing mice. The adenocarcinoma micro-CT image shows two mice with significant disease at low resolution, both small and large nodules (*white arrows*). The SCC micro-CT image shows two mice at high resolution. The image illustrates early (*right*) and late (*left*) stages of disease.

development of mouse lung SCCs, represent the first successful application of this novel mouse lung cancer model to chemoprevention studies. We also found that feeding ATB diet significantly reduced tumor development of adenomas and adenocarcinomas in both complete and progression protocols (10). Similarly, ATB was found to block the progression of bronchial cell hyperplasia and squamous metaplasia to SCC, as a higher percentage of hyperplasia were detected accompanied the decrease in lung SCCs. Thus, the efficacy of ATB on lung tumorigenesis is independent of tumor developmental stages.

Previously, we have shown that ATB displayed a significant reduction in benzo(*a*)pyrene-induced lung tumor multiplicity and tumor load in wild-type mice, mice harboring a dominant-negative p53, mice with heterozygous deletion of Ink4a/Arf, and mice with compound mutations (10). Taken together, these results provide important scientific evidence in support of clinical chemoprevention trials of ATB in

Downloaded from cancerpreventionresearch.aacrjournals.org on January 28, 2022. © 2009 American Association for Cancer Research.

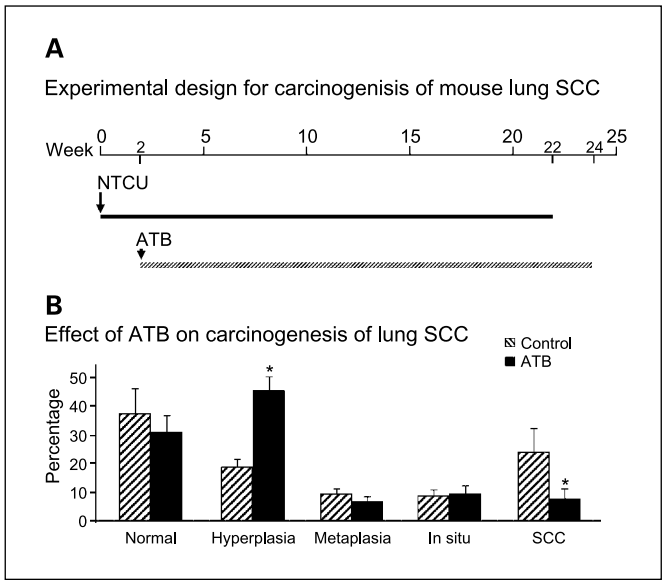

Fig. 3. Efficacy of ATB on development of lung SCC. *A*, design of the experiment. Chemoprevention by ATB of NTCU-induced lung SCCs in A/J mice is illustrated. Mice at age 6 to 8 wk were treated topically with 0.04 mol/L NTCU (*arrow*) twice a week for 22 consecutive wk. Two weeks after the start of NTCU treatment, mice were fed either AIN-76A Purified Diet # 100 000 or the same diet plus 250 g/kg ATB (*arrowhead*). Twenty-four weeks after the initial treatment of NTCU, mice were terminated by CO_2 asphyxiation. Horizontal lines, the time, by weeks, that mice were treated with carcinogen-control (*solid line*), or carcinogen + ATB (*shaded line*). *B*, efficacy of ATB on lung SCC development. Due to the difficulty to establish a tumor count on lung SCC with conventional approach as mouse SCC dose not form visible solid nodules on the surface of the lung, serial tissue sections were made from each formalin-fixed lung and 1 in every 20 sections was stained with H&E. To assess specific effects of these agents on each histopathologic stage, all of the bronchial in each given slides were counted and grouped into 5 categories based on normal, hyperplasia, metaplasia, SCC *in situ* (dysplasia was included in this category), and invasive SCC. The number in each category was then converted into percentage. *, $P < 0.05$.

patients with precancerous lesions of non–small cell lung cancer. This is because few agents have proven useful in preventing lung cancer to date. ATB is a promising candidate because it has been shown to inhibit effectively progression of precancerous lesions of human esophagus (dysplasia) to esophageal SCC (13).

We previously reported a chemically induced model for SCC of the lung in mice (16). The present study further showed that NTCU induction of SCC in mouse lung exhibits significant similarities to human lung SCC when comparing the histologic pictures of mouse lung SCC to that of human lung SCC (18). Distinguished histopathologic features in early (hyperplasia, squamous metaplasia), intermediate (dysplasia), and late (*in situ*, SCC) stages human lung SCCs are also seen NTCU-induced lung SCC. This similarity makes this mouse model ideal for testing chemopreventive agents in preclinical studies.

Next, we compared lung SCCs and adenocarcinomas using MRI and micro-CT. We believe that this is the first report of *in vivo* detection of primary lung SCCs in mice using either MRI or micro-CT imaging. Interestingly, lung adenocarcinomas were distributed randomly throughout the lungs, whereas early-stage SCCs were found to be more centrally located. At a later stage of disease, SCC lesions were distributed diffusely throughout the lungs. SCCs from both MRI and micro-CT showed continuous lesions, whereas adenomas or adenocarcinomas are more discreet. Our results indicate that MRI and micro-CT can clearly distinguish between adenocarcinoma and SCC and can be successfully applied for monitoring the effect of chemopreventive agents on lung tumor development and progression in mice. Longitudinal *in vivo* MRI/micro-CT are powerful modalities that can be of great aid in elucidating the factors that control the onset of lung tumors and can serve as a platform for the development and preclinical testing of novel therapies having a high likelihood of efficacy in human clinical trials.

Using oligonucleotide array analysis, we previously reported that ATB modulated as many as 114 genes belonging to several cellular signaling pathways, including G protein-Ras-MAPK (MAPK3, MAP3K4, rab3A, Rap1, RSG5, PKCh) and apoptosis (BAD, caspase 3; ref. 10). These results suggest that ATB may have a major effect on cell proliferation and cell cycle progression. We investigated the effect of ATB and its fractions on cell growth, cell cycle regulation, and activator protein activity in mouse cancer epithelial cells. Treatment with ATB and fractions A & B inhibit lung cancer epithelial cell growth, and arrested the cells at G_1 phase (Supplementary Data). Treatment of the cells with ATB and fractions A & B result in an inhibition of activator protein activity (Supplementary Data). These *in vitro* experiments showed that ATB caused cell growth inhibition, G_1 arrest, and activator protein inhibition.

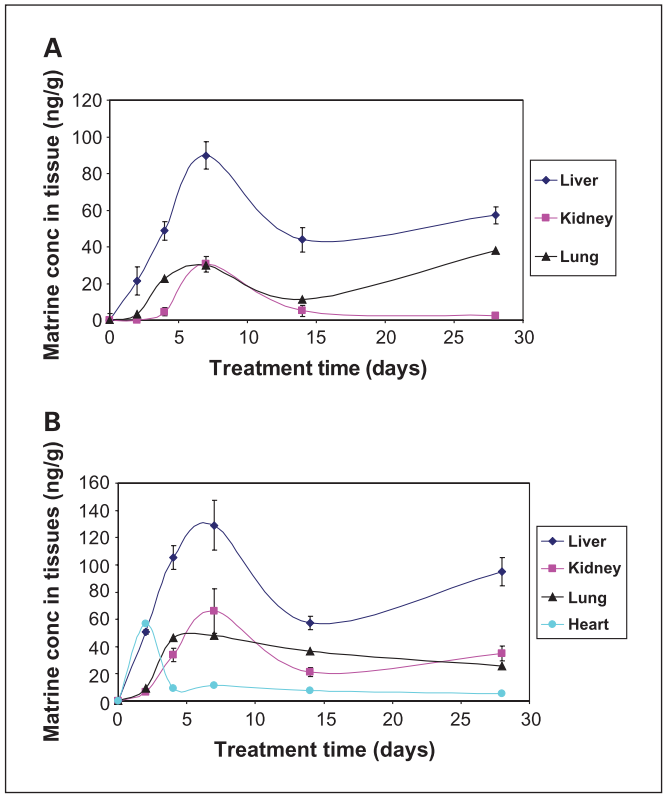

Fig. 4. Average tissue matrine concentration versus time profiles after feeding mice with ATB. *A*, 20% ATB in feeds; *B*, 30% ATB in feeds. The liver and kidney were extracted individually and each point represents the mean + SD of three mice. The heart and lung were combination from three mice and each point represents a single gas chromatograph/mass spectrometer-SIM analysis.

Downloaded from cancerpreventionresearch.aacrjournals.org on January 28, 2022. © 2009 American Association for Cancer Research.

In conclusion, ATB inhibits the development of lung SCC by blocking the progression of hyperplasia progression to SCC. ATB is rapidly absorbed and then distributes to various tissues including the lung. Mouse lung SCC exhibits significant similarities to human lung SCC. MRI and micro-CT can distinguish between adenocarcinoma and SCC and can be used to monitor tumor progression. Clearly, ATB is a potent chemopreventive agent against the development of mouse lung SCC in mice.

Disclosure of Potential Conflicts of Interest

No potential conflicts of interest were disclosed.

Acknowledgments

We thank Dr. Daolong Wang for statistical analysis on bioassay data and the members of Chemoprevention Group at The Siteman Cancer Center for careful reading of the manuscript.

References

1. Jemal A, Siegel R, Ward E, et al. Cancer statistics, 2008. CA Cancer J Clin 2008;58:71–96.
2. Hennekens CH, Buring JE, Manson JE, et al. Lack of effect of long-term supplementation with β carotene on the incidence of malignant neoplasms and cardiovascular disease. N Engl J Med 1996;334:1145–9.
3. Arnold AM, Browman GP, Levine MN, et al. The effect of the synthetic retinoid etretinate on sputum cytology: results from a randomised trial. Br J Cancer 1992;65:737–43.
4. Pastorino U, Infante M, Maioli M, et al. Adjuvant treatment of stage I lung cancer with high-dose vitamin A. J Clin Oncol 1993;11:1216–22.
5. Omenn GS, Goodman GE, Thornquist MD, et al. Risk factors for lung cancer and for intervention effects in CARET, the β-Carotene and Retinol Efficacy Trial. J Natl Cancer Inst 1996;88:1550–9.
6. Lee JS, Lippman SM, Benner SE, et al. Randomized placebo-controlled trial of isotretinoin in chemoprevention of bronchial squamous metaplasia. J Clin Oncol 1994;12:937–45.
7. van Zandwijk N, Dalesio O, Pastorino U, de Vries N, van Tinteren H. EUROSCAN, a randomized trial of vitamin A and N-acetylcysteine in patients with head and neck cancer or lung cancer. For the European Organization for Research and Treatment of Cancer Head and Neck and Lung Cancer Cooperative Groups. J Natl Cancer Inst 2000;92:977–86.
8. Lam S, MacAulay C, Le Riche JC, et al. A randomized phase IIb trial of anethole dithiolethione in smokers with bronchial dysplasia. J Natl Cancer Inst 2002;94:1001–9.
9. You M, Bergman G. Preclinical and clinical models of lung cancer chemoprevention. Hematol Oncol Clin North Am 1998;12:1037–53.
10. Zhang Z, Wang Y, Yao R, et al. Cancer chemopreventive activity of a mixture of Chinese herbs (antitumor B) in mouse lung tumor models. Oncogene 2004;23:3841–50.
11. Yan Y, Lu Y, Wang M, et al. Effect of an epidermal growth factor receptor inhibitor in mouse models of lung cancer. Mol Cancer Res 2006;4:971–81.
12. Yan Y, Wang Y, Tan Q, et al. Efficacy of polyphenon E, red ginseng, and rapamycin on benzo(a)pyrene-induced lung tumorigenesis in A/J mice. Neoplasia 2006;8:52–8.
13. Lin P, Zhang J, Rong Z, et al. Studies on medicamentous inhibitory therapy for esophageal precancerous lesions-3- and 5-year inhibitory effects of antitumor-B, retinamide and riboflavin. Proc Chin Acad Med Sci Peking Union Med Coll 1990;5:121–9.
14. Garbow JR, Zhang Z, You M. Detection of primary lung tumors in rodents by magnetic resonance imaging. Cancer Res 2004;64:2740–2.
15. Schuster DP, Kovacs A, Garbow J, Piwnica-Worms D. Recent advances in imaging the lungs of intact small animals. Am J Respir Cell Mol Biol 2004;30:129–38. Review.
16. Wang Y, Zhang Z, Yan Y, et al. A chemically induced model for squamous cell carcinoma of the lung in mice: histopathology and strain susceptibility. Cancer Res 2004;64:1647–54.
17. Sit DS, Gao G, Law FC, Li PC. Gas chromatography-mass spectrometry determination of matrine in human plasma. J Chromatogr B Analyt Technol Biomed Life Sci 2004;808:209–14.
18. Minna JD, Roth JA, Gazdar AF. Focus on lung cancer. Cancer Cell 2002;1:49–52. Review.
19. Gao GH (2007). Comparative Pharmacokinetics of Matrine: Pure Chemical vs. Crude Chemical in Acapha®. Ph.D. Thesis. Simon Fraser University.
20. Chang MY (1992). Anticancer Medicinal Herbs. Huamn Science and Technology Publishing House. Changsha, China.
21. Ma L, Wen S, Zhan Y, He Y, Liu X, Jiang J. Anticancer effects of the Chinese medicine matrine on murine hepatocellular carcinoma cells. Planta Med 2008;74:245–51.

Downloaded from cancerpreventionresearch.aacrjournals.org on January 28, 2022. © 2009 American Association for Cancer Research.

AACR American Association for Cancer Research

Cancer Prevention Research

Chemoprevention of Lung Squamous Cell Carcinoma in Mice by a Mixture of Chinese Herbs

Yian Wang, Zhongqiu Zhang, Joel R. Garbow, et al.

Cancer Prev Res 2009;2:634-640.

Updated version	Access the most recent version of this article at: http://cancerpreventionresearch.aacrjournals.org/content/2/7/634
Supplementary Material	Access the most recent supplemental material at: http://cancerpreventionresearch.aacrjournals.org/content/suppl/2009/07/13/2.7.634.DC1

Cited articles	This article cites 19 articles, 5 of which you can access for free at: http://cancerpreventionresearch.aacrjournals.org/content/2/7/634.full#ref-list-1
Citing articles	This article has been cited by 9 HighWire-hosted articles. Access the articles at: http://cancerpreventionresearch.aacrjournals.org/content/2/7/634.full#related-urls

E-mail alerts	Sign up to receive free email-alerts related to this article or journal.
Reprints and Subscriptions	To order reprints of this article or to subscribe to the journal, contact the AACR Publications Department at pubs@aacr.org.
Permissions	To request permission to re-use all or part of this article, use this link http://cancerpreventionresearch.aacrjournals.org/content/2/7/634. Click on "Request Permissions" which will take you to the Copyright Clearance Center's (CCC) Rightslink site.

Downloaded from cancerpreventionresearch.aacrjournals.org on January 28, 2022. © 2009 American Association for Cancer Research.